

Surface anisotropy and resonance modes in Co-SiO₂ heterogeneous films

J. Gómez and A. Butera*

Centro Atómico Bariloche and Comisión Nacional de Energía Atómica, Río Negro, Argentina

J. A. Barnard

Department of Materials Science and Engineering, School of Engineering, University of Pittsburgh, Pittsburgh, Pennsylvania 15261, USA

(Received 10 February 2004; revised manuscript received 23 March 2004; published 31 August 2004)

We have studied the magnetic properties of Co-SiO₂ films as a function of the Co concentration. Films were prepared using rf sputtering and Co volume concentrations in the range $0.18 \leq x \leq 0.62$ were obtained. The samples were measured using ferromagnetic resonance at X-band ($\nu=9.5$ GHz) and Q-band ($\nu=35$ GHz). A main absorption associated to the uniform precession of the magnetic moments was observed in all films. From this resonance field we have evaluated an effective anisotropy field (H_{eff}) as a function of x . For low Co concentrations the shape anisotropy is the major contribution to H_{eff} . However, above a critical concentration $x_p \sim 0.37$ (coincident with the percolation of the Co granules) it is necessary to assume the presence of an additional anisotropy to explain the experimental data. At this same concentration the resonance spectra change with the appearance of an extra absorption at fields higher than that of the uniform resonance mode. For larger Co concentrations another absorption is observed at intermediate fields. We have analyzed these extra lines using the surface inhomogeneity model that takes into account the different environment of the surface moments. The surface anisotropy was determined as a function of x with a behavior quite similar to the additional anisotropy obtained from H_{eff} . *In situ* annealing studies support the assumption that the observed behavior originates in the effects of the surface and suggest the nonequivalence of both film surfaces.

DOI: 10.1103/PhysRevB.70.054428

PACS number(s): 75.70.Ak, 76.50.+g, 81.05.Rm, 81.07.-b

I. INTRODUCTION

Physical systems in which one or more dimensions are confined generally have novel properties that are absent in their three dimensional counterparts. Heterogeneous, composite, or granular materials consist of metal granules embedded in an immiscible matrix. The relative ease of fabrication and their unique nanostructure made them ideal for studies of fundamental properties as a function of concentration, thickness, temperature dependence, etc. Chien and co-workers pioneered the work on magnetic granular systems, particularly in Fe-SiO₂.¹ They observed that below a critical (or percolation) concentration x_p , the magnetic grains tend to be single domain and usually exhibit hard magnetic properties dominated by dipolar coupling (if grains are too small they could be in superparamagnetic state). When the concentration is larger than x_p the exchange interaction among ferromagnetic (FM) grains dominates and the relatively soft properties of a continuous FM film are observed. The percolation threshold is thickness dependent in both metallic² and insulating matrices,³ with an average value $x_p \sim 0.40$ for a thickness of 100 nm. Co-SiO₂ has been less investigated than Fe-SiO₂. In particular no ferromagnetic resonance measurements of the surface modes have been made in these compounds as a function of concentration. The aim of this research is to perform a detailed study of the influence of film surface effects on the magnetic properties of heterogeneous Co-SiO₂ films.

II. SAMPLE PREPARATION AND EXPERIMENTAL SETUP

The samples were prepared using rf sputtering. The bottom half of an 8 in. diameter SiO₂ target was covered with a

Co foil. Two 2 in. square Corning 7059 glass substrates were placed one on top of the other facing the target. The following conditions were used during the sputtering process: base pressure 3×10^{-7} Torr, sputtering power 200 W, Ar pressure 10 mTorr. These conditions gave a sputtering rate of approximately 0.1 nm/s. A SiO₂ capping layer of 10 nm was sputtered to protect the films against oxidation. With the setup previously described it is possible to obtain a Co composition gradient along the vertical direction of approximately 0.5% vol/mm. The Co concentration as a function of the vertical distance was determined by EDAX analysis, which gives the atomic fraction of each element. We have used the density and the molecular weight of pure Co and SiO₂ to convert atomic concentrations to volume concentrations ($\delta_{\text{Co}}=8.9$ g/cm³, $\delta_{\text{SiO}_2}=2.2$ g/cm³). The obtained Co volume concentration ranged from 0.18 to 0.62. In Fig. 1 we show the plot of the Co concentration as a function of the vertical distance. The zero distance (where the two glass slides are joined) corresponds approximately to the center of the SiO₂-Co target. A stripe of 3 mm was cut along the vertical direction at the center of the substrates. This stripe was then cut in 34 pieces of $\sim 3 \times 3$ mm² that were used for the ferromagnetic resonance studies. In some cases (especially for large Co concentrations) smaller pieces needed to be used to prevent excessive loading of the resonant cavity. Due to the sputtering geometry and the fact that the yields of Co and SiO₂ are different, there is a small variation of the film thickness as a function of the vertical distance. All films used in this study have a thickness of 100 nm for $x=0.37$. For $x=0.62$ the thickness is 10% larger and for $x=0.18$ it is 25% smaller.

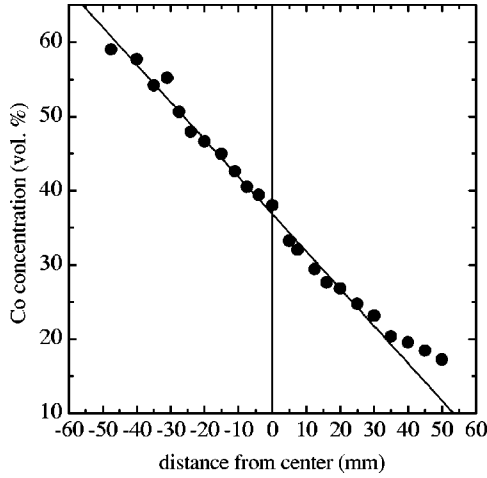


FIG. 1. Co volume concentration as a function of the vertical distance determined by EDAX spectroscopy. The straight line shows the approximately linear behavior, specially for large x .

Ferromagnetic resonance (FMR) measurements have been done with a commercial Bruker ESP 300 spectrometer at 35 GHz (Q-band) and 9.5 GHz (X-band) frequencies. The samples were placed at the center of a resonant cavity where the derivative of the absorbed power was measured using a standard field modulation technique (100 kHz frequency, 20 Oe amplitude). The Q-band resonator was a cylindrical cavity operating in the TM₁₁₀ mode, while the X-band resonator was a rectangular cavity operating in the TE₁₀₂ mode. The film plane was always parallel to the excitation microwave field and the dc external field changed from the in-plane to the out-of-plane direction. The maximum available dc field was 19 kOe. Measurements as a function of temperature were made using a dewar with a flow of hot nitrogen for temperatures up to 500 K and a special cavity with a quartz insert and a N₂-H₂ gas flow for higher temperatures.

III. MODEL, RESULTS, AND DISCUSSION

A. Uniform mode

1. Magnetic free energy

To describe the experimental data we propose three contributions to the magnetic free energy per unit volume: The Zeeman term that considers the interaction between the external field \mathbf{H} and the magnetization \mathbf{M} ; the demagnetization energy, imposed by the shape and the microstructure of the film; and a third term to consider the possible contribution of an easy plane or easy axis intrinsic anisotropy due to surface, magnetocrystalline, stress, or other sources of anisotropy but shape. The form of the magnetic free energy is then

$$F = -\mathbf{M} \cdot \mathbf{H} + \frac{1}{2} \mathbf{M} \cdot \underline{\mathbf{N}} \cdot \mathbf{M} + K_{\perp} \frac{(\hat{e}_{\perp} \cdot \mathbf{M})^2}{M^2}. \quad (1)$$

Here $\underline{\mathbf{N}}$ is the diagonal demagnetization tensor. We will assume that there is no in-plane anisotropy so that both parallel demagnetization factors are the same and $N_{\perp} + 2N_{\parallel} = 4\pi$. The anisotropy constant K_{\perp} could be either positive or negative

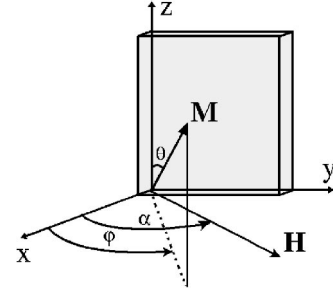


FIG. 2. Relative position of the film with respect to the axis and vectors. $\alpha=0^{\circ}$ corresponds to the external magnetic field \mathbf{H} applied perpendicular to the film plane.

to determine an easy plane or an easy axis of anisotropy, respectively. \hat{e}_{\perp} is a versor parallel to the film normal (the \hat{x} direction in the present geometry). The relative position of the film with respect to the axis and vectors is depicted in Fig. 2. When the magnetic field is applied in the xy plane, the expression for the free energy could be written as

$$F(\varphi, \alpha) = -HM \cos(\varphi - \alpha) - \frac{1}{2} H_{\text{eff}} M \sin^2 \varphi. \quad (2)$$

We have assumed that \mathbf{H} is large enough so that $|\mathbf{M}|$ is constant and the functional dependence is only on the angular variables. Additionally, if there is no in-plane anisotropy, the magnetization will lay on the xy plane and the azimuthal angle will be $\theta = \pi/2$. The angles φ and α can be related through the equilibrium condition for the magnetic free energy ($\partial F / \partial \varphi|_{\text{eq}} = 0$). The following relationship then holds:

$$H \sin(\varphi - \alpha) - \frac{1}{2} H_{\text{eff}} \sin 2\varphi = 0. \quad (3)$$

The effective field contains information about the sample anisotropy due to shape and other origins. It is defined as

$$H_{\text{eff}} = (N_{\perp} - N_{\parallel})M + 2K_{\perp}/M. \quad (4)$$

In continuous FM films, where the lateral dimensions are much larger than the thickness, N_{\parallel} can be taken as zero. However, in heterogenous films it was found that the shape of the individual grains is important when describing the overall magnetic behavior.⁴⁻⁶ For very low x there is very little interaction among magnetic grains, and each grain could be treated independently considering its own shape anisotropy. For larger concentrations, interactions among particles become important. Dipolar interactions first, and direct exchange for $x > x_p$ have an important influence on the demagnetization factor and the effective anisotropy field. For $x \ll x_p$ one would expect the demagnetization tensor to be an average of the demagnetization tensor of each grain ($\underline{\mathbf{N}}_g$), while for $x \gg x_p$ the continuous film demagnetization tensor ($\underline{\mathbf{N}}_f$) should be recovered, with $N_{\perp} = 4\pi$ and $N_{\parallel} = 0$. An approximate total demagnetization tensor is usually expressed as $\underline{\mathbf{N}} = (1-x)\underline{\mathbf{N}}_g + x\underline{\mathbf{N}}_f$.⁷ Note that the previous equation does not consider the effects of the dipolar interaction among grains (that becomes important for $x \geq 0.18$). This interaction could cause neighbor grains to act as a magnetic cluster so that the shape of the cluster instead of the individual grains should be considered. Rubinstein⁶ showed that in granular

thin films the effective value of magnetization to be used is the average or effective magnetization, which is a fraction of the saturation magnetization. For an ideal heterogeneous sample composed of spherical particles the magnetization should vary as $M = xM_s$ (M_s is the saturation magnetization) and then

$$H_{\text{eff}} = 4\pi x M_s + 2K_{\perp}/xM_s. \quad (5)$$

This expression proved to be correct,⁸ especially for $x > x_p$. It does not hold for small x because H_{eff} vanishes before $x=0$. Note that if shape were the only source of anisotropy a linear behavior of H_{eff} as a function of concentration is expected. Differences from a linear dependence are related to the appearance of additional anisotropy terms.

2. Determination of H_{eff} and the intrinsic anisotropy

The effective anisotropy field could be obtained from the out of plane angular variation of the resonance field. The Smit and Beljers equation,⁹

$$\left(\frac{\omega}{\gamma}\right)^2 = \frac{1}{M \sin^2 \theta} \frac{\partial^2 F}{\partial \varphi^2} - \frac{1}{M \sin \theta} \frac{\partial^2 F}{\partial \varphi \partial \theta},$$

is used to determine the dispersion relation for a given free energy. Applying the previous formula to Eq. (1) results in the following expression for the dispersion relation:

$$\left(\frac{\omega}{\gamma}\right)^2 = (H \cos(\varphi - \alpha) - H_{\text{eff}} \cos(2\varphi)) \times (H \cos(\varphi - \alpha) - H_{\text{eff}} \cos^2 \varphi). \quad (6)$$

From Eq. (6) and the equilibrium condition [Eq. (3)], it is possible to determine H_{eff} and the gyromagnetic factor g ($\gamma = g\mu_B/\hbar$) for a given concentration x and a frequency $\nu = \omega/2\pi$. The set of equations can be solved analytically only for $\alpha = 0^\circ$ (\mathbf{H} perpendicular to the film plane) and $\alpha = \pi/2$ (\mathbf{H} parallel to the film plane). For these angles the well known solutions due to Kittel¹⁰ (valid for $H_{\text{eff}} > 0$) are recovered:

$$\begin{aligned} \left(\frac{\omega}{\gamma}\right)^2 &= (H - H_{\text{eff}})^2 \quad (\alpha = 0^\circ), \\ \left(\frac{\omega}{\gamma}\right)^2 &= H(H + H_{\text{eff}}) \quad (\alpha = \pi/2). \end{aligned} \quad (7)$$

For other values of the angle α the equilibrium magnetization angle φ must be obtained numerically. In Fig. 3 we show a typical angular variation of the resonance field for $x = 0.375$ together with the numerically calculated best fit. For each sample a set of values for H_{eff} and g can be obtained which completely determine the free energy and the dispersion relation as far as the proposed model remains valid.

In Fig. 4 we present the concentration dependence of the effective field for X-band and Q-band, together with a straight line corresponding to the effective field of an ideal granular film with shape anisotropy only and magnetization $M = xM_s$. As H_{eff} is a parameter related to the sample properties, it should not depend on the working frequency. However, in Fig. 4 it is observed that for small x the values

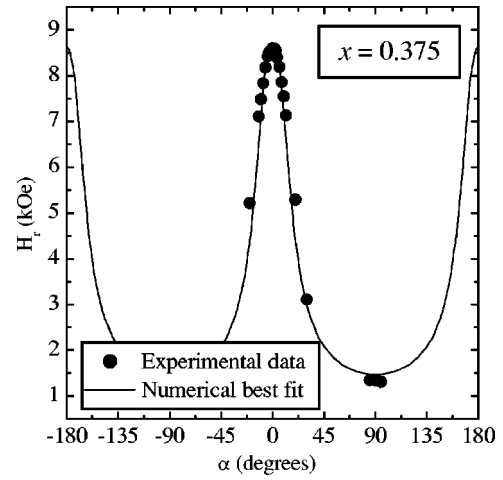


FIG. 3. Typical variation of the resonance field as a function of the angle formed between H and the film normal. Full circles correspond to the experimental data and the continuous line is the numerically calculated best fit. Measurements were made at X-band on a sample with a Co concentration $x = 0.375$.

obtained from measurements at Q-band are larger than the values obtained from X-band data, while for $x > 0.5$ both effective fields tend to be coincident as previously observed⁴ in Fe-SiO₂. The discrepancy for low concentrations is attributed to the nonsaturation of the magnetization at the field values in which resonance occurs at X-band⁸ (especially for $\alpha \sim \pi/2$). The field dependence of $|\mathbf{M}|$ is not considered in the present model and corrections to the calculated values of H_{eff} from X-band data should be made. To confirm that $|\mathbf{M}|$ is not saturated at the fields where resonance occurs at X-band, we measured a few M vs H loops in a VSM magnetometer. We have found that for \mathbf{H} parallel to the film plane complete saturation is only obtained for $H \geq 4000$ Oe for $x < 0.5$. Typical values of the resonance fields for $\alpha = \pi/2$ are $H_r \sim 1000$ Oe for which M is about 70% of satu-

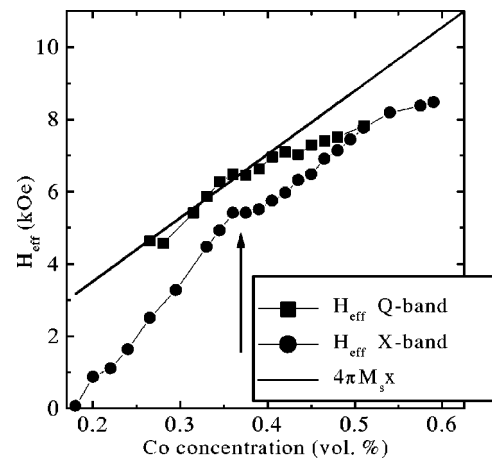


FIG. 4. Effective anisotropy field as a function of the Co volume concentration. Circles correspond to X-band data and squares to Q-band measurements. The continuous line corresponds to the effective field of an ideal film with magnetization $M_s x$ and only shape anisotropy. The arrow indicates the Co concentration where a change in behavior is observed.

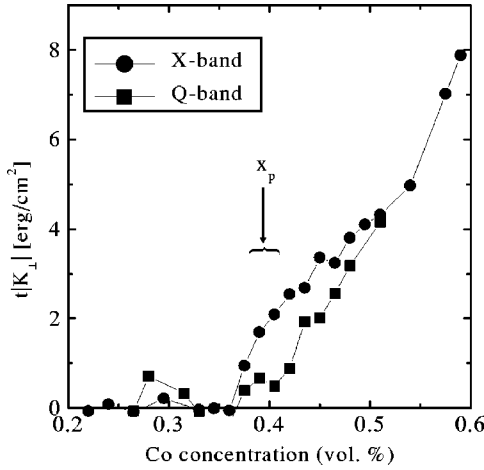


FIG. 5. Absolute value of the anisotropy constant as a function of Co concentration for Q-band (squares) and X-band (circles). The anisotropy is negative indicating the existence of an easy axis perpendicular to the film plane. Values have been normalized by the film thickness $t \sim 100$ nm. The arrow indicates the range where magnetic percolation occurs in ~ 100 nm thick heterogeneous films (Ref. 3).

ration. Q-band resonance fields are always larger than 8000 Oe for all orientations of α and hence the experimental results are better described by the proposed model. Unfortunately, perpendicular resonance for Co-rich samples at Q-band occurs at fields larger than the maximum available magnetic field and H_{eff} for $x > 0.5$ could not be calculated using 35 GHz data.

The g value could be also obtained from the fitting of the angular variation of the resonance field. The values obtained from Q-band measurements are almost concentration independent with an average value $\langle g \rangle = 2.195$, coincident with the g value of FM bulk Co ($g_{\text{Co}} = 2.18 - 2.22$).¹¹ g values obtained from X-band data show large fluctuations and values considerably different than the accepted g_{Co} , probably as a consequence of the nonsaturation of $|\mathbf{M}|$.

For concentrations close to $x = 0.37$ there is a change in the shape of the H_{eff} vs x curve for both Q-band and X-band data. This value of x is very close to the percolation concentration in granular systems ($x_p \sim 0.40$). Note that for $x < x_p$ the values of H_{eff} obtained from Q-band data follow the curve $H_{\text{eff}} = 4\pi M_s x$ indicating that shape is the only source of anisotropy in Eq. (5). H_{eff} values obtained from X-band data also decrease linearly and go to zero for $x = 0.18$. For $x > x_p$ the H_{eff} curve lies below $H_{\text{eff}} = 4\pi M_s x$ indicating that an additional anisotropy appears above this concentration. The anisotropy constant K_{\perp} is negative, tending to align the magnetization perpendicular to the film plane. The appearance of this additional anisotropy at the percolation concentration suggests that it is related to the exchange interaction that begins to dominate for $x > x_p$. From the difference between the extrapolated linear behavior and the calculated H_{eff} we have estimated K_{\perp} , the anisotropy values (normalized by the film thickness) are presented in Fig. 5. The values calculated from X-band data have been obtained assuming that K_{\perp} is zero for $x < x_p$ and that H_{eff} preserves its linear behavior until $x \sim 0.45$ where it becomes parallel to the curve $4\pi M_s x$.

B. Additional absorptions

At the same concentration where the H_{eff} vs x curve has a kink ($x \sim 0.37$) an additional resonance line appears at fields larger than that of the uniform mode with the following characteristics: The separation between both lines is maximum for $\alpha = 0^\circ$ and they merge at a critical angle α_c ; both α_c and the maximum separation at $\alpha = 0^\circ$ depend on x ; the critical angle is larger for Q-band than for X-band; for large x another additional absorption is observed at intermediate fields.

1. Model

The excitation of surface modes could be described using the surface inhomogeneity (SI) model.¹² In this model the effects of the surface energy on the boundary conditions and the magnetization inhomogeneities in the region close to the surface are explicitly considered. First of all it is necessary to introduce an extra energy term that accounts for the variation of \mathbf{M} with position,¹³ $F_p = -(A/M^2)\mathbf{M} \cdot \nabla^2 \mathbf{M}$. Then the total magnetic free energy is now written as:

$$F = -\mathbf{M} \cdot \mathbf{H} + \frac{1}{2} \mathbf{M} \cdot \mathbf{N} \cdot \mathbf{M} + K_{\perp} \frac{(\hat{e}_{\perp} \cdot \mathbf{M})^2}{M^2} - \frac{A}{M^2} \mathbf{M} \cdot \nabla^2 \mathbf{M}. \quad (8)$$

Here A is the exchange stiffness constant that is directly proportional to the exchange integral J . Assuming an oscillatory behavior for \mathbf{M} with wave vector k parallel to the film normal (\hat{x} direction in Fig. 1), the free energy can be written as a function of the angular variables,

$$F(\varphi, \alpha) = -HM \cos(\varphi - \alpha) - \frac{1}{2} H_{\text{eff}} M \sin^2 \varphi + Ak^2, \quad (9)$$

which is similar to Eq. (2) except for a factor Ak^2 arising from the spatial variation of \mathbf{M} . The Smit and Beljers relation can be generalized in the case $k \neq 0$,¹⁴

$$\left(\frac{\omega}{\gamma}\right)^2 = \left(\frac{1}{M \sin^2 \theta} \frac{\partial^2 F}{\partial \varphi^2} + \frac{2A}{M} k^2\right) \left(\frac{1}{M} \frac{\partial^2 F}{\partial \theta^2} + \frac{2A}{M} k^2\right) - \left(\frac{1}{M \sin \theta} \frac{\partial^2 F}{\partial \varphi \partial \theta}\right)^2.$$

If we apply the previous formula to Eq. (9) the dispersion relation now becomes

$$\left(\frac{\omega}{\gamma}\right)^2 = \left(H \cos(\varphi - \alpha) - H_{\text{eff}} \cos(2\varphi) + \frac{2A}{M} k^2\right) \times \left(H \cos(\varphi - \alpha) - H_{\text{eff}} \cos^2 \varphi + \frac{2A}{M} k^2\right). \quad (10)$$

The preceding expression is the general solution of the equation of motion for arbitrary k . The values of k will depend on the conditions at the surface and will be determined by the surface boundary conditions.

2. Boundary conditions and allowed wave vectors

We will use the following boundary conditions first proposed by Rado and Weertman:^{15,16}

$$\begin{aligned}\partial_n m_\theta + p m_\theta + r m_\varphi &= 0, \\ \partial_n m_\varphi + q m_\varphi + r m_\theta &= 0,\end{aligned}\quad (11)$$

where

$$\begin{aligned}p &= \frac{1}{2A} \frac{\partial^2 F_s}{\partial \theta^2} - \frac{\partial_n M}{M}, \\ q &= \frac{1}{2A} \left(\frac{\cos \theta}{\sin \theta} \frac{\partial F_s}{\partial \theta} + \frac{1}{\sin^2 \theta} \frac{\partial^2 F_s}{\partial \varphi^2} \right) - \frac{\partial_n M}{M}, \\ r &= \frac{1}{2A} \left(-\frac{\cos \theta}{\sin^2 \theta} \frac{\partial F_s}{\partial \varphi} + \frac{1}{\sin \theta} \frac{\partial^2 F_s}{\partial \varphi \partial \theta} \right).\end{aligned}\quad (12)$$

Here m_θ and m_φ are the transverse components of M proportional to $e^{i(\omega t + kx)}$, ∂_n represents the spatial derivative normal to the film plane, and F_s is the free energy per unit volume associated with the surface anisotropy. The quantities p , q , and r must be evaluated at both surfaces ($x=0$ and $x=L$) so that in principle four equations are obtained from Eq. (11). In order to search for the allowed wave vectors we rewrite Eq. (10) as

$$\Omega^2 = (P + Dk^2)(Q + Dk^2), \quad (13)$$

with $P = H \cos(\varphi - \alpha) - H_{\text{eff}} \cos(2\varphi)$, $Q = H \cos(\varphi - \alpha) - H_{\text{eff}} \cos^2 \varphi$, $D = 2A/M$, and $\Omega = \omega/\gamma$. Two solutions are obtained for the wave vector k^2 ,

$$Dk_{1,2}^2 = -\frac{P+Q}{2} \pm \sqrt{\left(\frac{P-Q}{2}\right)^2 + \Omega^2}. \quad (14)$$

The plus and the minus signs correspond to k_1^2 and k_2^2 , respectively. For $\alpha \sim 0^\circ$ the resonance field is always larger than H_{eff} so that the quantity $P+Q$ is positive. This means that k_1^2 could be either positive or negative (and then k_1 could be real or imaginary), and k_2 is always imaginary. Solutions for real k , called standing spin waves, are interpreted as waves propagating in the direction perpendicular to the film plane and correspond to volume modes. When k is imaginary the solution corresponds to surface waves that are attenuated inside the film. Note that the two solutions are related by the condition $Dk_2^2 = Dk_1^2 + (P+Q)$. This means that $|k_2| > |k_1|$, and because k_2^2 is negative it corresponds to waves that are attenuated much faster than those corresponding to k_1 . In the single wave-vector approximation¹⁶ the normal modes for the dynamic microwave magnetization are assumed to be generated only by k_1 (which will be called k from now on). The spatial dependence of m_θ and m_φ is then of the form

$$\begin{aligned}m_\theta &= A_0 \sin(kx) + A_1 \cos(kx), \\ m_\varphi &= A_2 \sin(kx) + A_3 \cos(kx).\end{aligned}\quad (15)$$

3. Surface modes and spin waves

In order to apply the SI model we need to assume a form for the surface free energy F_s . For simplicity we propose the following phenomenological expression:

$$F_s = K_s \cos^2 \varphi \sin^2 \theta, \quad (16)$$

where K_s is the surface anisotropy constant. This surface free energy can describe both an anisotropy causing an easy axis perpendicular to the film plane ($K_s < 0$) or an easy plane coincident with the film plane ($K_s > 0$). Note that the additional modes are only observed when the field is close to the film plane normal ($\alpha \sim 0^\circ$). In this situation the angle of the magnetization vector of the uniform mode φ_u is very similar to the angle corresponding to the additional mode φ_s . The separation between both angles is zero for $\alpha = 0^\circ$ and $\alpha = \alpha_c$, and has a maximum at an intermediate angle. In our case $\Delta\varphi = (\varphi_s - \varphi_u)_{\text{max}} < 0.5^\circ$ for Q-band measurements and $\Delta\varphi < 3^\circ$ for X-band measurements, so that in general we will use $\varphi_u = \varphi_s = \varphi$. For simplicity we will also assume that for $\alpha \sim 0^\circ$ we can approximate $\cos(2\varphi) = \cos^2 \varphi - \sin^2 \varphi \sim \cos^2 \varphi$. With these approximations we obtain from Eq. (12),

$$p = q = \left(\frac{K_s}{A} \cos(2\varphi) - \frac{\partial_n M}{M} \right)_{x=0,L}, \quad r = 0. \quad (17)$$

The boundary conditions [Eq. (11)] now take the form

$$\partial_n m_\theta + \left(\frac{K_s}{A} \cos(2\varphi) - \frac{\partial_n M}{M} \right)_{x=0,L} m_\theta = 0. \quad (18)$$

The differential equation for m_φ is similar to Eq. (18). Replacing Eq. (15) into Eq. (18) and evaluating at both film surfaces we obtain the following:

$$\begin{aligned}A_0 k \cos(kL) - A_1 k \sin(kL) + A_0 p_L \sin(kL) + A_1 p_L \cos(kL) \\ = 0 \quad \text{for } x=L, \quad -A_0 k + A_1 p_0 = 0 \quad \text{for } x=0.\end{aligned}\quad (19)$$

In the above equations p_0 and p_L indicate the value that the quantity $[(K_s/A)\cos(2\varphi) - (\partial_n M/M)]$ takes at $x=0$ and $x=L$, respectively. Equation (19) has a nonzero solution when the determinant formed by the coefficients A_0 and A_1 is equal to zero, i.e., $(p_0 p_L - k^2) \sin(kL) + (p_0 + p_L) k \cos(kL) = 0$. Two solutions are obtained for the wave vector k ,

$$\tan(kL) = \frac{(p_0 + p_L)k}{k^2 - p_0 p_L} \quad \text{if } k \text{ is real}, \quad (20)$$

$$\tanh(k_s L) = -\frac{(p_0 + p_L)k_s}{k_s^2 + p_0 p_L} \quad \text{if } k = ik_s \text{ is imaginary}. \quad (21)$$

The parameters p_0 and p_L have information of the surface anisotropy and the variation of the magnetization on both surfaces. They are equal for films with symmetric surfaces and differ if the conditions at both surfaces are not the same. In the case of real k the solutions correspond to volume spin waves. For large anisotropy and symmetric conditions the Kittel solutions for standing spin waves are obtained.¹⁷ For other conditions Eq. (20) must be solved numerically.

When k is imaginary the solutions are obtained from the intersection of the two curves of Eq. (21). For symmetric surface conditions only one intersection may exist, while for asymmetric surfaces up to two different wave vectors can be found. In both cases larger values of the anisotropy constant

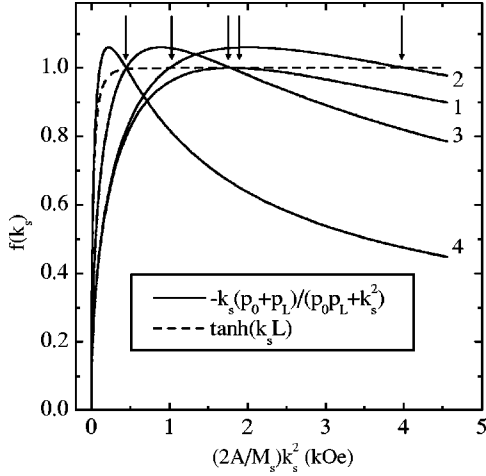


FIG. 6. Plot of the functions of Eq. (21) for symmetric (curve labeled 1) and asymmetric (curves 2 to 4) conditions at both surfaces. The intersections (marked with arrows) are the allowed values for the wave vector of the surface waves. At most one intersection can be found in the symmetric case while up to two solutions can be obtained for asymmetric surfaces. For simplicity we have set $\partial_n M = 0$. We used the following values of the surface anisotropy constant: curve 1, $|K_s| = 2 \text{ erg/cm}^2$; curve 2, $|K_s(x=0)| = 0.5 \text{ erg/cm}^2$, $|K_s(x=L)| = 1 \text{ erg/cm}^2$; curve 3, $|K_s(x=0)| = 1 \text{ erg/cm}^2$, $|K_s(x=L)| = 2 \text{ erg/cm}^2$; curve 4, $|K_s(x=0)| = 1.5 \text{ erg/cm}^2$, $|K_s(x=L)| = 3 \text{ erg/cm}^2$.

K_s cause a larger k_s . Another property of the surface modes is that Eq. (21) has solutions only for negative K_s , which then defines an easy axis anisotropy perpendicular to the film plane. In Fig. 6 we show schematically the cases of equal ($p_0 = p_L$) and unequal ($p_0 \neq p_L$) surfaces. The possible intersections of the two curves correspond to the wave vectors that are solutions of Eq. (21). For the parameters involved in the present model the function $\tanh(k_s L)$ rapidly takes the value 1, even for small K_s . Equation (21) can then be approximated, $1 \sim \tanh(k_s L) = -(p_0 + p_L)k_s / (k_s^2 + p_0 p_L)$. This implies that

$$k_{s1} = p_0, \quad k_{s2} = p_L, \quad \text{if } p_0 \neq p_L, \quad (22)$$

$$k_s = p, \quad \text{if } p = p_0 = p_L.$$

If we make again the approximation $\cos(2\varphi) \sim \cos^2 \varphi$ (valid for small angles where the additional resonances are observed) the dispersion relation Eq. (10) could be written as

$$\frac{\omega}{\gamma} = H \cos(\varphi - \alpha) - H_{\text{eff}} \cos(2\varphi) + \frac{2A}{M} k^2. \quad (23)$$

Note that Eq. (23) reduces to Eq. (6) for $k=0$ and $\alpha \sim 0^\circ$. For $k \neq 0$ it is observed that a real k produces resonance fields lower than the uniform mode and that for imaginary k the surface modes have a resonance field larger than that of the uniform mode. In the limit $\alpha \sim 0^\circ$ we have the following equations for the resonance fields of the uniform and the surface modes,

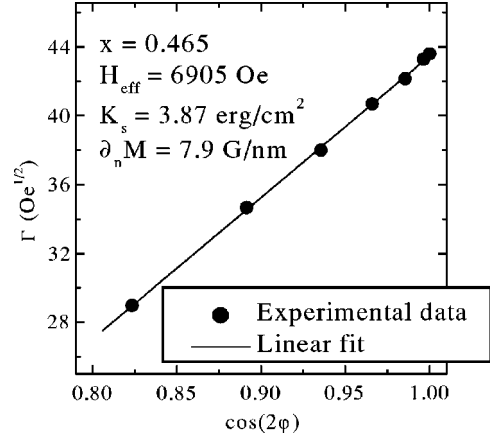


FIG. 7. Γ vs $\cos(2\varphi)$ for the sample with a volume concentration $x=0.465$ and $H_{\text{eff}}=6905 \text{ Oe}$ (solid circles). From the linear fit we have extracted the values of the parameters K_s and $\partial_n M$ indicated on the figure. Data has been taken from X-band measurements.

$$\frac{\omega}{\gamma} = H_u \cos(\varphi_u - \alpha) - H_{\text{eff}} \cos(2\varphi_u), \quad (24)$$

$$\frac{\omega}{\gamma} = H_s \cos(\varphi_s - \alpha) - H_{\text{eff}} \cos(2\varphi_s) - \frac{2A}{M} k_s^2. \quad (25)$$

H_u and H_s are the resonance fields of the uniform and the surface modes, respectively. In the present approximation $\varphi_s \cong \varphi_u = \varphi$, so that subtracting the preceding equations we get $\sqrt{(H_s - H_u)} \cos(\varphi - \alpha) = \sqrt{2A/M} |k_s|$. Remembering that $k_s = p$ in the symmetric case and that $k_{s1} = p_0, k_{s2} = p_L$ in the asymmetric situation, we could use Eq. (17) to write

$$\Gamma = \sqrt{(H_s - H_u) \cos(\varphi - \alpha)}$$

$$= \sqrt{\frac{2}{AM}} |K_s|_{0,L} \cos(2\varphi) - \sqrt{\frac{2A}{M}} \frac{\partial_n M}{M}. \quad (26)$$

As Γ must be always positive there is a critical angle for which the uniform and the surface modes are coincident, $\cos(2\varphi_c) = (A/K_s)(\partial_n M/M)$.

4. Experimental results

In Fig. 7 we have plotted the quantity Γ as a function of $\cos(2\varphi)$ for the sample with $x=0.465$. The linear dependence between both quantities is a good indication that the additional absorption corresponds to a surface resonance mode. If we assume that the exchange stiffness constant A is the same as for bulk Co (Ref. 18) ($A_{\text{Co}} = 3.2 \times 10^{-6} \text{ erg/cm}$, see Ref. 19). We can obtain the surface anisotropy constant and the parameter $\partial_n M$ from the linear fit of the data of Fig. 7. Both parameters can then be estimated as a function of the Co concentration. In Fig. 8(a) we show the values of K_s as a function of concentration together with the values of the total anisotropy K_\perp multiplied by the film thickness. K_s is zero for low concentrations where a single resonance line is observed and increases as a function of x . The larger values of K_s for larger x come from the fact that the separation between H_u

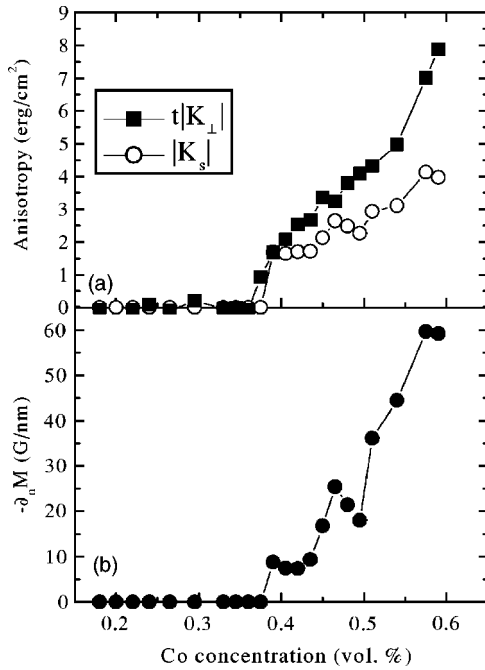


FIG. 8. (a) Comparison between the total anisotropy $t|K_{\perp}|$ and the surface anisotropy $|K_s|$ as a function of the Co concentration x . (b) Dependence of the parameter $-\partial_n M$ as a function of the Co concentration x . Data calculated from X-band measurements.

and H_s (for $\alpha=0^\circ$) increases with the Co concentration. As x increases the exchange interaction among FM grains is larger and the magnetization is more affected by the conditions at the surface. In the case of symmetric surfaces we expect an increase in the separation between both lines, but we do not expect a second additional absorption. Although we are not completely sure, we believe that we are in the asymmetric case because for $x \geq 0.52$ a second mode appears at intermediate fields. The difference between the two resonance fields, $H_{s2} - H_u$, also increases with increasing x . This fact suggests that for a given concentration the conditions at both surfaces change in such a way that two different solutions are allowed in Eq. (21). This interpretation implies that both surfaces are not equivalent, probably because of a different environment (the glass substrate is not necessary the same as the SiO_2 capping layer) or some degree of oxidation in the top layer. The anisotropy constant of the second surface mode could not be calculated because it was very close to the uniform mode and the superposition of both lines prevented a good estimation of the resonance field.

We have also calculated the parameter $\partial_n M$. This quantity is related to the change in magnetization at the surface region. A larger value of $\partial_n M$ indicates a sharper surface (i.e., the transition from bulk magnetization to surface magnetization is more abrupt). The observed dependence with concentration confirms that the surface is sharper for larger x [see Fig. 8(b)]. This result is again a consequence of the increasing exchange interaction among Co grains. Note that the values of $\partial_n M$ are negative, as it should be for a film in which the magnetization decreases towards the film surface.

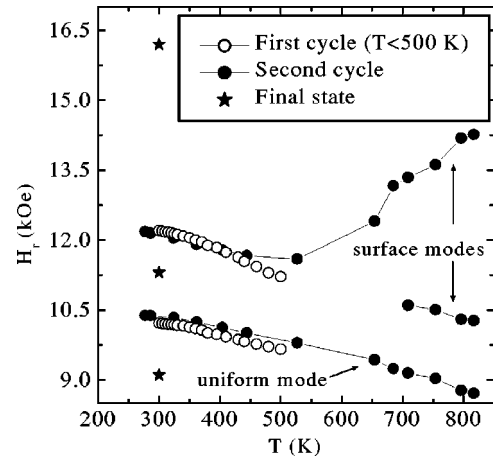


FIG. 9. Temperature variation of the uniform and the surface modes during the first sequence (open circles), during the second sequence (solid circles), and at room temperature after the last cycle (solid stars). Measurements were made at X-band, in a sample with a Co concentration $x=0.48$, and for $\alpha=0^\circ$. Note the irreversible changes after both temperature cycles.

Measurements in Fe-SiO₂ films²⁰ showed the presence of surface modes for a single Fe concentration ($x=0.42$). The parameters K_s and $\partial_n M$ calculated for Fe granular films are of the same order of magnitude than our results in Co, supporting the validity of the employed model.

C. Temperature dependence

To study the effects of temperature we selected a sample with a concentration above the percolation threshold ($x=0.48$). At room temperature (T_R) this sample has only one surface mode. Below room temperature no significant changes occurred, but when the temperature was raised the spectra changed considerably. Consequently we concentrated the measurements in this temperature region. In the first temperature sequence we raised T from T_R up to 500 K. We measured the resonance field of the uniform and the surface modes for $\alpha=0^\circ$. The results are shown in Fig. 9 with open circles. It is observed that both resonance fields decrease at high temperatures. This result is associated to the decrease of M with T in FM materials. The perpendicular resonance field is proportional to H_{eff} [see Eq. (7)], which is dominated by shape effects and is essentially proportional to M . There is also a decrease in the separation between H_u and H_s with temperature indicating a decrease in the surface wave vector k_s .

After the first temperature cycle we made another measurement from T_R to 800 K. We would like to stress that the initial conditions were not the same. In Fig. 9 we have plotted the results of this second sequence as full circles. It is observed that the mode separation at T_R is smaller and that the value of H_u is slightly larger. These differences indicate that the thermal treatment, even at moderated temperatures, is enough to produce irreversible changes to the sample. The increase of H_u at T_R originates in a larger value of M , probably due to the release of tensions or the better definition of the grain surfaces after the sample was heated. When the

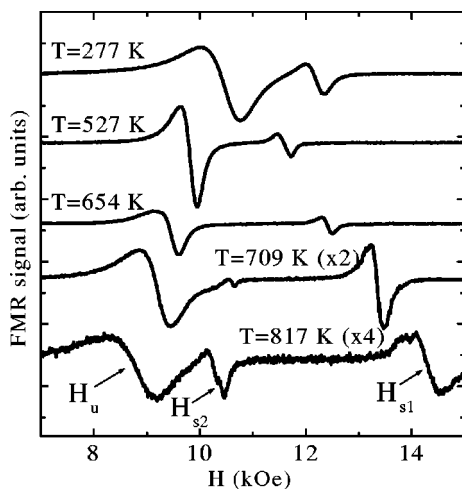


FIG. 10. Resonance spectra for the sample with $x=0.48$ measured during the second temperature cycle. The uniform mode and the two surface modes are indicated by arrows. Measurements have been done at X-band with the magnetic field perpendicular to the film plane ($\alpha=0^\circ$). The y-axis scale of the two spectra at the bottom of the figure has been amplified by the factor in parentheses.

sample was heated for the second time the separation $H_u - H_s$ remained constant up to 500 K as can be seen in Fig. 9. The fact that the two measurements gave different results is due to a change in the sample properties *during* the first measurement. In the second cycle the state reached after the first temperature sequence stayed frozen and no structural changes occurred up to 500 K. Above 500 K the behavior of the surface mode changed. In this region H_s increased with increasing temperature. From ~ 700 K a second surface mode appears between the two previously observed absorptions.

In Fig. 10 we show a sequence of spectra measured at different temperatures corresponding to the second temperature cycle. The growth of a second surface mode is clearly observed and the sudden increase in the resonance field of the first surface mode becomes evident for $T > 500$ K. The appearance of a second surface mode is a clear indication that we are in a situation of asymmetric boundary conditions. In this case the temperature caused a different effect on both surfaces favoring the observation of a second line. Back to room temperature the second surface line did not disappear, the uniform mode resonance was reduced to 9 kOe and the surface mode position reached 16 kOe (see Fig. 9, solid stars). This again indicates that the sample suffered irreversible changes, but this time not only related to the microstruc-

ture but probably to grain diffusion or chemical changes (in spite of the capping layer, the exposed Co surface could have oxidized at these high temperatures). We have used the formalism of Sec. III B 3 to calculate the surface anisotropy constant and $\partial_n M$ (at room temperature), and we have obtained the following values: $|K_{s1}| = 28.9$ erg/cm², $|\partial_n M_1| = 1040$ G/nm; $|K_{s2}| = 3.17$ erg/cm², $|\partial_n M_2| = 139$ G/nm. Within the proposed theoretical framework these results indicate that there is an increase in the surface anisotropy after the thermal treatment. We have not yet a definitive explanation for this increase, but it is evidently favored by the irreversible changes produced by the thermal cycles. A similar behavior was observed in annealed Fe/Ni multilayers.²¹

IV. CONCLUSIONS

We have determined the anisotropy of Co-SiO₂ heterogeneous films using FMR measurements. From the field position of the uniform mode we have calculated the effective anisotropy field and estimated the total anisotropy constant K_\perp . We have observed that K_\perp is zero for low x and starts to grow above the critical or percolation concentration x_p . At this concentration the ferromagnetic grains begin to form a continuous network and the exchange interaction becomes dominant over other interactions. As a consequence the film surfaces start to be well defined. At this same value of x we have observed a new resonance line at fields larger than H_u . This line merges with the uniform mode line at a critical angle α_c and there is also a linear relationship between the quantity Γ and $\cos(2\varphi)$. These characteristics are typical of surface resonance modes arising from the different conditions at the film surface. We have estimated the value of the surface anisotropy as a function of x from the angular variation of the additional resonance line. K_s follows the same trend as K_\perp but with lower values (see Fig. 5) suggesting that it contributes considerably to the total anisotropy. Differences may arise from the presence of other anisotropies that we did not consider in the present model, or to small variations of the parameters A or M_s taken from measurements made in bulk Co. We have observed a second additional line both at large concentrations or when the films are heated above 700 K. The appearance of this extra absorption suggests that both film surfaces are not equivalent.

ACKNOWLEDGMENTS

The authors wish to acknowledge the support of ANPCyT, Argentina, through Grants Nos. PICT 03-3392 and PICT 36340, and Conicet, Argentina through Grant No. PIP 2626.

*Also at Consejo Nacional de Investigaciones Científicas y Técnicas, and Instituto Balseiro–Universidad Nacional de Cuyo, Argentina; Electronic address: butera@cab.cnea.gov.ar

¹C. L. Chien, *Annu. Rev. Mater. Sci.* **25**, 129 (1995), and references therein.

²A. Butera, T. J. Klemmer, and J. A. Barnard, *J. Appl. Phys.* **83**,

4855 (1998).

³J. N. Zhou, A. Butera, H. Jiang, and J. A. Barnard, *J. Appl. Phys.* **84**, 5693 (1998); J. N. Zhou, A. Butera, H. Jiang, D. H. Yang, and J. A. Barnard, *ibid.* **85**, 6151 (1999).

⁴A. Butera, J. N. Zhou, and J. A. Barnard, *Phys. Rev. B* **60**, 12 270 (1999).

- ⁵U. Neztelmann, J. Appl. Phys. **68**, 1800 (1990).
- ⁶M. Rubinstein, B. N. Das, N. C. Koon, D. B. Chrisey, and J. Horwitz, Phys. Rev. B **50**, 184 (1994); M. Rubinstein, J. Tejada, and X. X. Zhang, J. Appl. Phys. **75**, 6557 (1994).
- ⁷G. N. Kakazei, A. F. Kravets, N. A. Lesnik, M. M. Pereira de Azevedo, Yu. G. Pogorelov, and J. B. Sousa, J. Appl. Phys. **85**, 5654 (1999).
- ⁸N. A. Lesnik, C. J. Oates, G. M. Smith, P. C. Riedi, G. N. Kakazei, A. F. Kravets, and P. E. Wigen, J. Appl. Phys. **94**, 6631 (2003).
- ⁹J. Smit and H. G. Beljers, Philips Res. Rep. **10**, 113 (1955).
- ¹⁰C. Kittel, Phys. Rev. **73**, 155 (1948).
- ¹¹B. Cullity, *Introduction to Magnetic Materials* (Addison-Wesley, New York, 1972), p. 125.
- ¹²H. Puzskarski, Prog. Surf. Sci. **9**, 191 (1979).
- ¹³C. Vittoria, *Microwave Properties of Magnetic Films* (World Scientific, Singapore, 1993), p. 71.
- ¹⁴L. J. Maksymowicz and H. Jamkowski, J. Magn. Magn. Mater. **109**, 341 (1992).
- ¹⁵G. Rado and J. Weertman, J. Phys. Chem. Solids **11**, 315 (1959).
- ¹⁶A. Maksymowicz, Phys. Rev. B **33**, 6045 (1986).
- ¹⁷C. Kittel, Phys. Rev. **110**, 1295 (1958).
- ¹⁸This is not always the case. Chien has found that in Fe granular films the constant A is lower than in continuous films. C. L. Chien, J. Appl. Phys. **69**, 5267 (1991).
- ¹⁹R. Pauthenet, J. Appl. Phys. **53**, 2029 (1982).
- ²⁰W. N. Wang, Z. S. Jiamg, and Y. W. Du, J. Appl. Phys. **78**, 6679 (1995).
- ²¹R. Kordecki, R. Meckenstock, J. Pelzl, and S. Nikitov, J. Appl. Phys. **73**, 6359 (1993).